Experimental investigation on convective heat transfer enhancement by EHD in wire to plate configuration

Merouane Hamdi, Olivier Rouaud, Dominique Tarlet, Michel Havet

Journal Pre-proofs

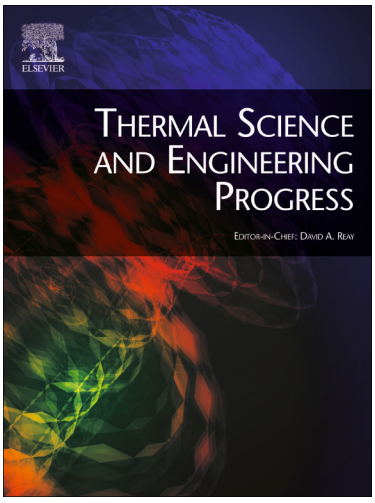

Experimental investigation on convective heat transfer enhancement by EHD in wire to plate configuration

M. Hamdi, O. Rouaud, D. Tarlet, M. Havet

PII: S2451-9049(21)00247-X
DOI: https://doi.org/10.1016/j.tsep.2021.101086
Reference: TSEP 101086

To appear in: *Thermal Science and Engineering Progress*

Received Date: 30 May 2021
Revised Date: 16 September 2021
Accepted Date: 18 September 2021

Please cite this article as: M. Hamdi, O. Rouaud, D. Tarlet, M. Havet, Experimental investigation on convective heat transfer enhancement by EHD in wire to plate configuration, *Thermal Science and Engineering Progress* (2021), doi: https://doi.org/10.1016/j.tsep.2021.101086

Experimental investigation on convective heat transfer enhancement by EHD in wire to plate configuration

M. Hamdi[a], **O. Rouaud**[a], **D. Tarlet**[b], **M. Havet**[a]

a. *Oniris, Université de Nantes, CNRS, GEPEA, UMR 6144, F-44000 Nantes, France*

b. *Laboratoire de Thermique et Énergie de Nantes (LTeN), CNRS UMR 6607, Polytech Nantes, rue C. Pauc, BP 50609, 44306 Nantes, France*

Keywords: Electrohydrodynamics, PIV, Convective heat transfer, Forced convection

Abstract

The purpose of this study was to experimentally investigate the enhancement of forced convection heat transfer by corona wind in a channel scaled to potential future drying systems. An experimental rig was designed to investigate the thermal and dynamic effects of electro-hydrodynamic (EHD) induced air flow on the grounded bottom wall. The primary air flow, blown into the channel at controlled temperature and velocity, was disturbed by EHD secondary flow generated by a wire electrode. Using IR imaging, the heat transfer exchange at the wall was calculated in several configurations (i.e. electrodes location, wire-electrode to plate distance, applied voltage, primary air flow velocity), allowing the selection of optimal configurations according to the objective of minimum energy consumption or homogeneous transfer. Particle Image Velocimetry (PIV) characterization conducted on some configurations highlighted the vortices generated by the combination of the secondary and the primary air flows. Analysis of the flow patterns allowed to explain the enhancement of the local and average heat transfer coefficients. Higher enhancement could be obtained in the cross-wire configuration but led to heterogeneous treatment. For a more homogeneous one, the longitudinal wire configuration should be preferred thanks to the development of contra-rotating vortices moving in the channel.

Nomenclature

A	Surface area	[m^2]
b	Ion mobility	[$m^2.V^{-1}.s^{-1}$]
d	Inter –electrode spacing	[cm]
h	Heat transfer coefficient	[$W.m^{-2}.K^{-1}$]
I	Electric current	[A]
L	Length	[m]
N_{EHD}	EHD number	[-]
P	Electric power	[W]
Re	Reynolds number	[-]
ρ	Air density	[$kg.m^{-3}$]
T	Temperature	[°C]
U	Velocity	[$m.s^{-1}$]
U_∞	Primary mean flow velocity	[$m.s^{-1}$]
V	Voltage	[V]

Subscripts

0	reference
amb	ambient
i	threshold
loc	local
m	mean
p	plate
s	secondary
sup	polystyrene support
top	top
wire	wire
x	refer to x axis
y	refer to y axis
z	refer to z axis

Abbreviations

EHD: Electro Hydro Dynamic

PIV: Particle Image Velocimetry

DBD: Dielectric barrier discharge

IR: Infrared

1. Introduction

One of the most promising techniques to enhance convective heat transfer in air is based on the use of the Electrohydrodynamic (EHD) induced air flow. The basic principle of EHD is the mechanism by which an electric field is used to influence the flow pattern. The effect can be carried out by corona discharge to induce flow motion (ionic wind) using either AC or DC high voltages.

Since EHD induced flows do not use any mechanical moving parts, they are of great interest and can be used in many thermal engineering applications. The advantages of using EHD technique include the reduction in size of the facility, improved control of thermal characteristics by monitoring the electrical field intensity, and simplicity in setting up due to the minimal requirements [1]. Moreover, their fast response and simplicity make them more attractive as the electric energy is converted simply into kinetic energy and many studies have demonstrated the excellent potential of EHD as a technology for improving the energy efficiency of thermal systems. [2–6].

Several studies have been carried out concerning the use of EHD in process engineering. Large varieties of geometrical configurations, operating parameters and working fluid have been the subject of numerical and experimental investigations. EHD flows have been much investigated for their potential applications as flow actuators [7] or electrohydrodynamic thrust [8], in heat exchangers [9] and cooling devices [10], for electrosprays [11], collecting particles [12] or corona-enhanced chemical reactions [13]. Some studies such as [14] and [15] demonstrated the ability of corona discharges to reduce drag by modifying the boundary layer.

The use of EHD in the presence of a bulk flow to alter an external boundary layer has been an area of growing interest in the aerospace community while has received little attention for heat transfer enhancement. However, studies on this subject have shown that the increase in the heat transfer coefficient can be high depending on the configuration. For example the increase can reach 250% for a heated plate in air [16], 270% in a wire / plate configuration [17] and up to 830% for HCFC-123 boiling application [5]. A list of relevant studies using EHD in process engineering applications, dealing with heat transfer enhancement, is presented in Table 1.

90 **Table I** Some studies carried out on the use of EHD in processes specifically dedicated to heat transfer
91 enhancement, with varying electrodes configurations and working fluids.

Reference	Type of research	Fluid	Electrode shape	Application
[17–19]	Experimental	Air	wire / plate	Convective heat transfer
[19,20]	Numerical	Air	wire / plate	
[16,21]	Experimental	Air	multi-wires / plate	
[21,22]	Numerical	Air	multi-wires /plate	
[3]	Experimental	Air	needle-array / plate	
[23–25]	Experimental	Air	wire / tube	
[26]	Experimental	Air	Multi-rod / plate	
[27,28]	Numerical	Air	wire / cylinder	
[29]	Experimental	Air	wire / tube and 2 wires / tube	
[30]	Experimental	Air	needle / meshed plate	
[10]	Experimental	Air	wire / semi-cylindrical contour	
[31]	Experimental	Air	wire / triangular tube	
[32]	Experimental	Fe3O4 / ethylene glycol	wire / wire	
[19]	Experimental / Numerical	Oil	wire / plate	
[6,33–36]	Experimental	Air	wire / plate	Drying
[37]	Numerical	Air	wire / plate	
[4]	Numerical	Air	multi-wires / plate	
[38]	Numerical	Air	wire / mesh and periodic wire / mesh	
[39,40]	Experimental	Air	single-pin, needle / plate	
[41–43]	Experimental	Air	multi-pin, multi-needle / plate	
[44]	Experimental	Air	needle / wire	
[45]	Experimental	Air	multi-pin/wire	
[46]	Experimental	HFC-134a	wire / inner tube wall	Condensing systems
[47]	Experimental/ Theoretical	HCFC-123	wire / inner tube wall	
[1]	Experimental	HFC-134a	wire / inner tube wall	
[48]	Experimental	HFC-134a	rod / inner tube wall	
[49]	Experimental	HFC-245fa	rod / inner wall	
[50]	Experimental	HCFC-123	concentric wire / cylinder	Boiling systems
[51]	Experimental	HFC-134a	concentric wire / cylinder	
[52]	Experimental	HFE 7000	rod / inner tube wall	
[5]	Experimental	HCFC-123 and CFC-11	rod / tube wall	
[53]	Experimental	N-pentane	rod / cylinder sheet	
[2]	Experimental	HCFC-123	wire mesh / tube wall	
[54]	Numerical	liquid CCl4	wire / wire	
[55]	Experimental	NaCl solutions	pin / plate	Evaporating systems
[56]	Experimental	HFC-134a	wire mesh / rectangular ribs	
[57,58]	Numerical	Water	wire / plate	
[59]	Experimental	HCFC-123 and HCFC-141b	plate multilayered /plate	

[9]	Experimental	HFE-7000	wire / inner tube wall	

Many studies deal mainly with natural convection flow [19,21,31,32], and are rarely focused on the forced convection flow. Velkoff and Godfrey [16] reported the first experiments on heat transfer enhancement by ionic winds in the presence of external flows. They demonstrated that the heat transfer was enhanced in the low-velocity regime; however, the ionic wind was swamped by the bulk flow. Thus, it was ineffective as the bulk velocity increases. A wide range of studies either experimental [18,26,29,30], and numerical [4,20,22,28] have been conducted using EHD for heat transfer intensification in a channel. These studies have shown that the most effective EHD-induced flow can be achieved by lowering the bulk flow velocity.

Moreover, the EHD phenomenon in a channel depends on various parameters such as Reynolds number and applied voltage. The EHD is also a function of geometrical aspect such as the number of electrodes, the distance between electrodes, the wire radius, and the characteristics of the channel [60]. It can be noticed that many questions regarding the optimization of the operating parameters remain unanswered while the control of heat transfer remains a key factor for many industrial applications.

During the past decade, EHD has undergone a growing interest in aerodynamic induced secondary flow in drying process. The literature points out that the EHD-induced flow has widely attracted the researchers' attention and they developed assisted-drying processes [37,39,42–44]. Compared to conventional hot air forced convective drying systems and freeze-drying, EHD drying systems in a channel can improve the energy efficiency by reducing energy consumption. Increasing locally, the heat and mass transfer lead to the reduction of the high inlet velocity of the drying air. This contributes to a significant reduction of the energy consumption in the whole drying process.

As reported by Kudra and Martynenko [61], EHD drying was recognized as an energy efficient and environmentally friendly technique: the drying time was reduced by about 15-40% with a drying rate multiplied by 1.3 to 4.52, depending on the operating conditions, type of material and amount of humidity in the sample. Ould Ahmedou et al [60] have shown that the ionic wind generated by a corona discharge could lead to weight losses equivalent to those resulted from forced convection at 4.2 $m.s^{-1}$. They concluded that EHD drying process is a promising alternative to enhance heat and mass transfer. Lai [35] was one of the first to demonstrate that EHD technology could be scaled up from laboratory bench to industrial size. The results revealed that the drying enhancement by corona wind in real applications depends on many

124 factors such as corona polarity, electrode spacing and height, conveyor moving velocity,
125 characteristics of material, etc. He concluded that an accurate tune of these factors is necessary to
126 optimize the operating conditions of the system. Regarding the electrode configuration, one can
127 notice from Table 1, that wire-plate and point-plate configuration are widely used. Lai and Wong
128 [40] have found that the wire / electrode configuration was more suitable in EHD drying when
129 compared to the needle at smaller values of supplied voltage. Defraeye and Martynenko [38],
130 based on a numerical study, recommended the wire-to-mesh configuration for drying because the
131 configuration provides a more uniform drying. It is however difficult to generalize these results
132 as the electrodes configurations also depend on the drying process type (continuous or batch…)
133 and the majority of studies have been conducted with small-size prototypes.

134 Given the simple design and reduced energy consumption, drying systems based on EHD
135 enhanced heat transfer demonstrate a promising potential for bulk and industrial drying
136 applications, especially for heat-sensitive products [62]. Nevertheless, as already raised [36,63],
137 the main obstacle is the up-scaling and optimization of the EHD process and its associated
138 system. For this reason, a parametric analysis is crucial to determine how the governing
139 parameters affect the heat transfer rate in EHD drying applications.

140 Therefore, this paper focuses on both thermal and flow structure characterization for EHD
141 induced secondary flow inside a semi-industrial scale channel using wire to plate
142 configuration. Combining both Infrared (IR) thermal imaging and Particle Imaging
143 Velocimetry (PIV) measurement technics, the influence of geometrical and operating
144 parameters involved in the process were evaluated, with the aim to optimize the heat transfer
145 intensification ratio to energy consumption.

146 Local and average convective heat transfer coefficients were calculated from the surface plate
147 temperature measured by the IR system. Using air velocities resulting from PIV post-processing,
148 the vortex structures generated by the interaction of secondary flow and primary flow were
149 related to the heat transfer intensification. The effect of the inlet air velocity, the influence of
150 geometrical parameters such as arrangement of wire-electrodes (parallel or perpendicular to
151 primary air flow), wire-electrode to plate distance (d) and applied voltage (V) were investigated
152 and discussed. From an analysis of energy consumption in each configuration, optimal
153 configurations were selected. Since the final application of this study is dedicated to drying
154 process, the analysis was extended by taking into consideration other criteria such as the
155 homogeneity of the heat transfer coefficient.

To our knowledge, this work is one of the first where both PIV and IR imaging were used in a semi-industrial scale channel to analyze heat transfer enhancement due to EHD secondary air flow.

2. Material and methods

2.1. Experimental Set-up

The experimental set-up consisted of a rectangular channel section (15 cm × 19 cm) as shown in **Fig.1**. Air flow was introduced into the channel at a controlled humidity using an Air Handling Unit (Munters ML 180, France). The inlet air temperature was adjusted by a cooling unit (Hitema, Italy) and the primary air flow velocity U_∞ was controlled by valves. A honeycomb filter was placed at the entrance of the channel to stabilize the air flow. The investigation area, i.e the plate, had dimensions of 15 cm × 15 cm and was mounted flush to the bottom wall of the channel 100 cm downstream from the inlet. Electrically heated, the surface of the plate was considered to evaluate the heat transfer coefficient. The heat was supplied by Joule effect using a DC power supply (EL302, 30V 2A). A stainless-steel wire electrode (Ø =0.2 mm) was placed in the flow channel over the plate. To induce the ionic wind, a positive corona discharge was applied to the wire using a high voltage supply (High voltage supplier, Spellman, USA). **Fig.1** also shows two configurations for wire electrode arrangement, parallel and cross-wire. For the parallel arrangement, the wire electrode was placed parallel to the primary flow direction, while the wire was oriented across the air flow in the cross-wire arrangement. For both arrangements, different values for inter-electrode gap, *d*, were considered.

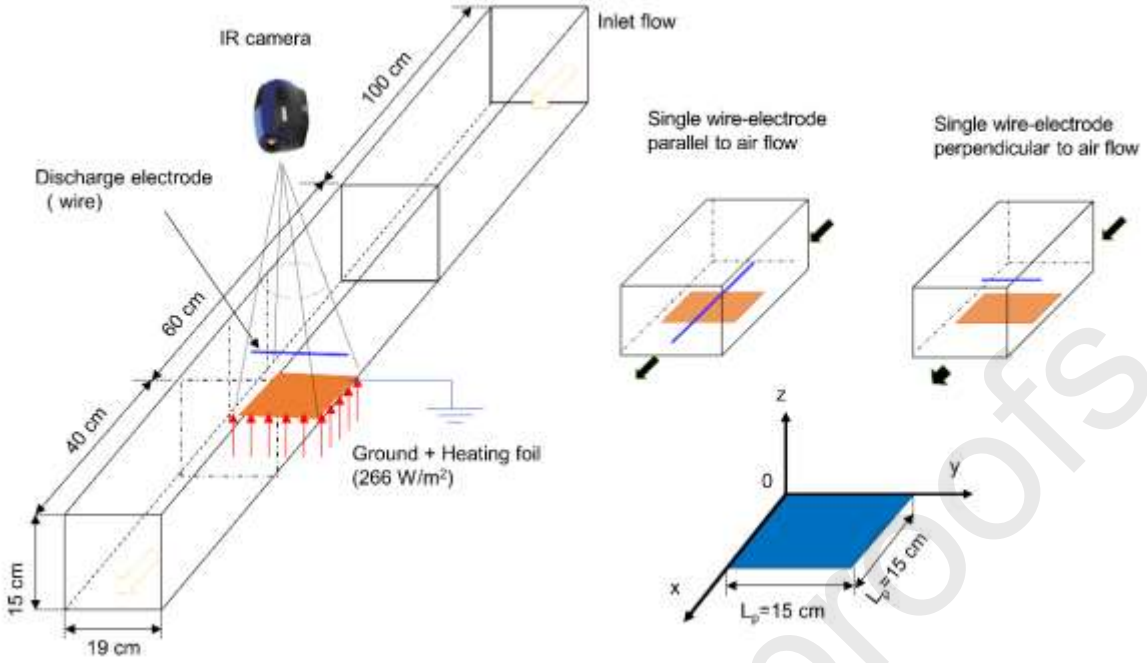

Figure 1. *Schematic diagram of the experimental setup and arrangement of electrodes*

A humidity sensor (Vaisala HMT100, Finland), was placed right before the outlet to measure the humidity of the air flow in the channel. A velocity sensor (Velocicalc 9545, TSI, USA) was also introduced into the channel through an opening at the upper wall to measure the mean velocity of primary flow at the start of the investigation area. Moreover, temperature at different locations in the channel and the plate were recorded using several K type thermocouples. All the above-mentioned instruments were connected to a data logger (AOIP Datalog S20, France) where the measurements were acquired and recorded for further processing.

2.1.1. Thermal instrumentation

The heating plate, shown in **Fig. 1,** consisted of a heating foil (17.02 Ω) insulated on both sides by a thin layer of Kapton (50 µm) and covered with a 30 µm aluminum layer on the upper face. The surface was used as both the ground electrode and the heat transfer surface. This surface was painted matt black (Electrotube, France) in order to achieve an emissivity close to 1. The assembly was placed on a 4 cm thick polystyrene insulating plate. The temperature field of the plate was measured with an infrared camera (Silver 450M Cedip, France) in the range of 3-5 µm. The camera had an accuracy of ±0.01 °C with a spatial resolution of 0.428 mm/pixel. The acquisition frequency was chosen at 50 Hz with a maximum resolution of 1280×800. The control and data recording of the camera were provided by a specific software. The camera

was installed on a vertical support and adjusted vertically at the correct focal distance. A rectangular box, made with thick black matt paper, was placed between the camera and the channel to avoid reflections. Temperature measurement was conducted through a circular opening of 12 cm diameter at the top wall of the channel. To avoid air escaping from the channel, which could have affected the heat transfer on the surface plate, the hole was covered with a plastic foil, transparent at the working wavelength, and positioned at an angle > 35° to avoid any reflections. The circular opening did not provide access to the temperature of the heating plate corners. The cross section shown in **Fig.2** illustrates the thermal instrumentation in the cross-wire arrangement.

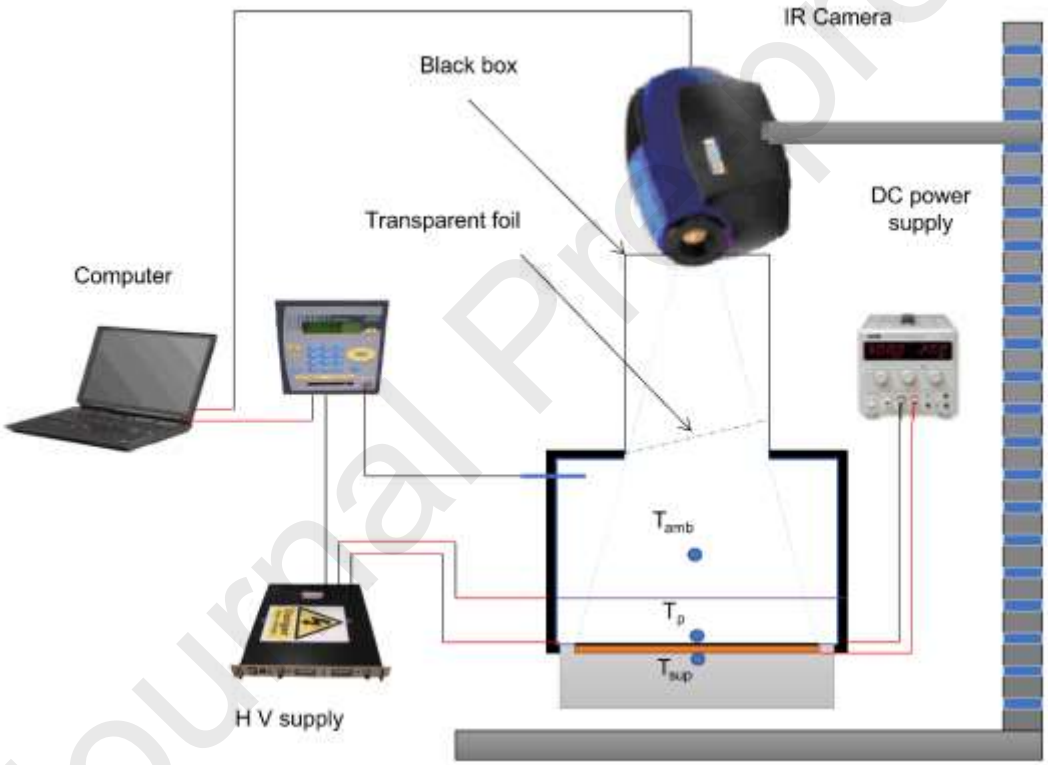

Figure 2. *Cross-sectional view of the experimental set-up in cross wire-electrode configuration*

Prior the beginning of the acquisition, about 15 minutes waiting time was required to allow the thermal equilibrium of the heating plate to be reached. By performing an energy balance under uniform heat flux, the local and mean steady-state heat transfer coefficients were evaluated from the local surface temperature and the mean temperature, respectively.

2.1.2. PIV Instrumentation

The experimental rig used above was adapted for 2D PIV measurements by making some technical modifications. Close to the investigation area, the upper and lateral walls were replaced by glass walls of 4 mm thickness. The main flow entered the viewing area and passed over the upper surface of the plate. The same reference point *xyz* defined in **Fig.1** was retained. Measurement in the *xz* plan was performed by positioning the laser sheet parallel to the primary flow and perpendicular to the plate. The camera (Flow-Sens, Dantec Dynamics, Denmark), focused in the direction of the *y*-axis and was placed perpendicularly to the laser sheet as shown in **Fig. 3-a**. For measurement in *yz* plan, the laser sheet was generated in the direction of the *y*-axis perpendicular to the primary flow while the camera was placed at the outlet channel in the direction of *x*-axis as shown in **Fig. 3-b**.

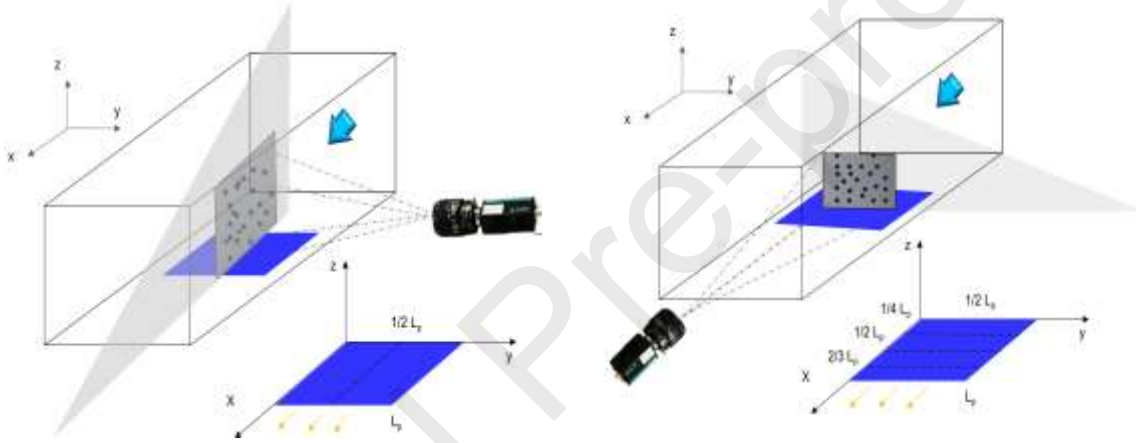

a) *Measurement in the xz configuration plan* ***b*)** *Measurement in the yz configuration plan*

Figure 3. *PIV measurement in the xz and yz configuration plans*

The flow seeding was carried out by incense particles of diameter of 0.8 µm [64]. To generate seeding a combustion box was designed and placed at the air intake channel where several incense sticks were burned simultaneously. As reported in [64], seeding the flow with incense smoke particles is suitable for EHD flows. The particles concentration in the channel was measured by an optical particle counter (Grimm: model G1.10, Austria) and was of the order of 10^5 particles.L^{-1}, giving a particles density suitable for PIV measurement. The values of the measurement parameters are shown in **Table II.**

Table II. PIV acquisition parameters

Acquisition frequency	5 Hz
Number of snapshots	300
Size of the interrogation area	32×32
Time between two laser pulses	300 µs
Post-processing algorithm	Adaptive correlation

3. Results and discussions

For the purpose of heat transfer optimization in the channel, energy balance must be performed. The heat flux generated by Joule effect in the heating plate is mainly evacuated by convection with air through the upper face. The remaining heat is evacuated by irradiation with the channel walls and conduction through the downwardly polystyrene. The local and mean heat transfer coefficient respectively designated by h_{loc} and h_m were calculated for different configurations with the change in the electric power consumed P *(W)* for EHD generation. The power P was defined from the current and the voltage ($P = V\,I$).

The EHD number "N_{EHD}" introduced by [65] was defined by relation (1) which expresses the ratio of electrostatic forces to the inertial forces. This number is interesting to characterize the EHD flow configuration.

$$N_{EHD} = \frac{U_s}{U_\infty} = \frac{I L_{wire}}{\rho b A_p {U_\infty}^2} \tag{1}$$

The secondary flow velocity U_s was estimated from the experimentally measured electrical current value. Analytical relationship to calculate the velocity is given by equation (2). This relationship is described in the literature by [66] and [67].

$$U_s = \left[\sqrt{\frac{I L_{wire}}{\rho b A_p}}\right] \tag{2}$$

Experimental investigations for varying arrangement of wire-plate electrode under different values of the mean primary flow velocity U_∞ and the applied voltage V have been conducted. **Table III** shows either cross wire and longitudinal wire configurations under varying primary flow velocity, electrode gap and applied voltage.

Table III. Experimental configurations

Configuration	Primary air flow Velocity U_∞ *(m/s)*	Electrode gap *d (cm)*	Voltage *V (kV)*
Cross wire	*0.3*	*2*	*0 to 11*
	0.6	*4*	*0 to 18*
	1.0	*6*	*0 to 20*
Longitudinal wire	*0.3*	*2*	*0 to 11*
	0.6	*4*	*0 to 16*
	1.0	*6*	*0 to 18*

From **Table III**, it can be noticed that the maximum applied voltage was limited due to the electrical arcing which mainly depends on the electrode gap. In the case of cross wire configuration and primary flow velocity of 0.3 m.s^{-1} (*Re* = 3525), **Fig.4** shows the corresponding current voltage characteristic curve for three different electrode gaps.

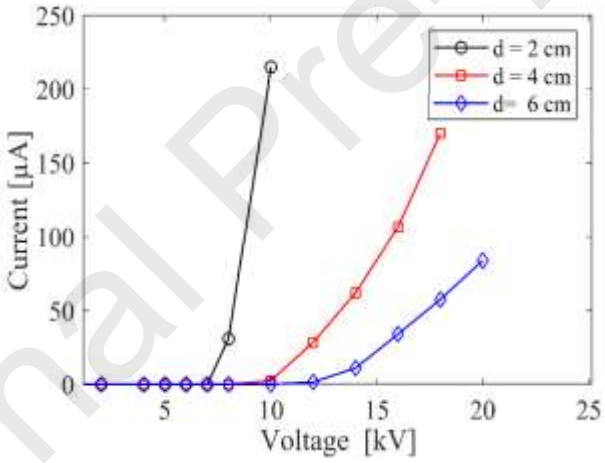

Figure 4. *Current-Voltage characteristic curve in cross wire configuration for varying electrode gap (U_∞ = 0,3 m.s^{-1})*

Increasing the electrode gap (from d = 2 cm to d = 6 cm), led to the increase of the corresponding threshold voltage (from V_i = 7.8 kV to Vi =12 kV). As the electrode gap increased, the slope of the increase on current/voltage decreased and the value of the voltage limit increased. As a result, the corona discharge application range increased.

3.1. Temperatures and heat transfer enhancement

Fig.5 shows the temperature distribution on the plate given by infrared thermal camera images of both cross wire (**5a-c)** and longitudinal wire (**5e-g)** configurations for varying electrode gap and for a primary air flow velocity $U_\infty = 0.3$ *m/s*. The blue vertical (**5a-c**) or horizontal (**5e-g**) lines in these figures correspond to the location of the wire electrode. It can be distinguished easily that the cooling of the plate mainly took place in portions just beneath the wire. When comparing between cross wire configuration and longitudinal wire, it can be noticed that in longitudinal wire the cooling effect was more homogeneous compared to the cross-wire case.

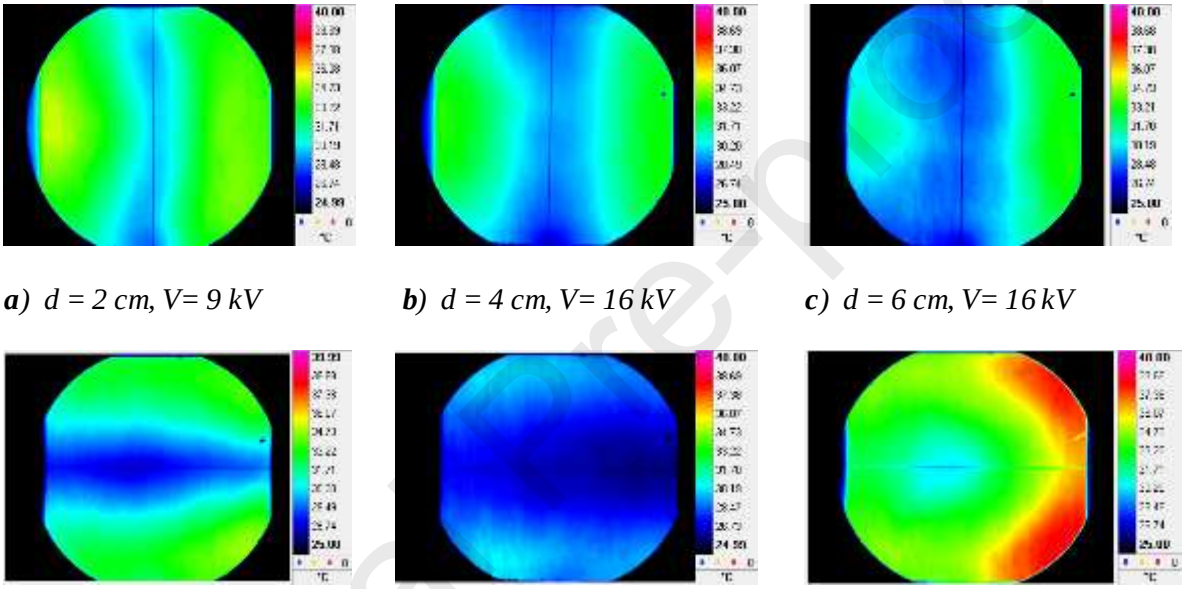

***a**) d = 2 cm, V= 9 kV* ***b**) d = 4 cm, V= 16 kV* ***c**) d = 6 cm, V= 16 kV*

***e**) d = 2 cm, V= 9 kV* ***f**) d = 4 cm, V= 16 kV* ***g**) d= 6 cm, V= 16 kV*

***Figure 5**. Temperature distribution mapping of: **(a,b,c)** cross-wire configuration and **(e,f,g)** longitudinal wire configuration for $U_\infty = 0.3$ m/s.*

Because the power supplied to the plate may be slightly different between each experiments, as well as air temperature, it was not possible to evaluate the heat transfer enhancement directly from the temperature distribution. Only the determination of the mean heat transfer coefficient makes it possible the comparison of the different configurations.

Fig.6 and Fig.7 displays the evolution of the mean heat transfer coefficient h_m as a function of the power consumption in cross wire and longitudinal wire configurations, respectively, for three primary air flow velocities.

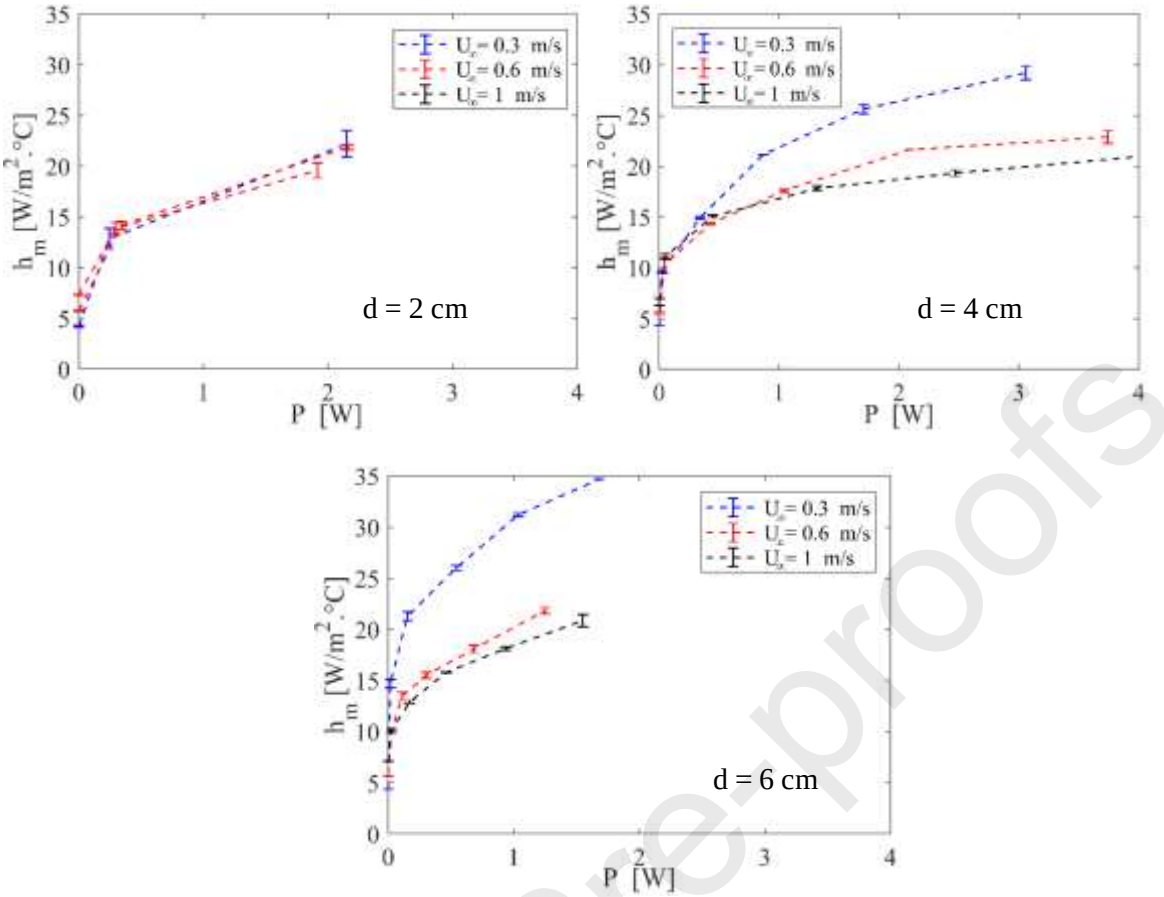

293

294

295 ***Figure 6.*** *Evolution of the mean heat transfer coefficient (h_m) as a function of power consumption in cross*
296 *wire configuration*

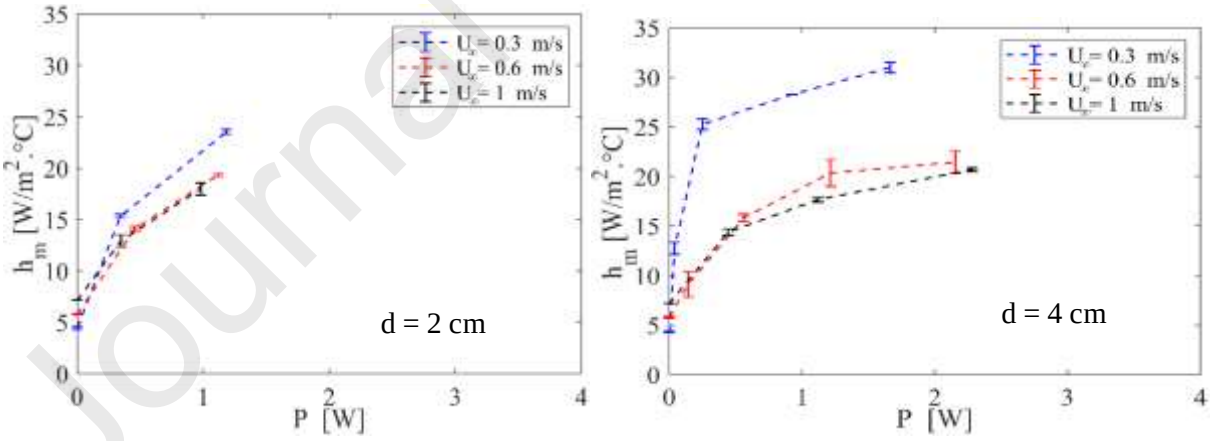

297

298

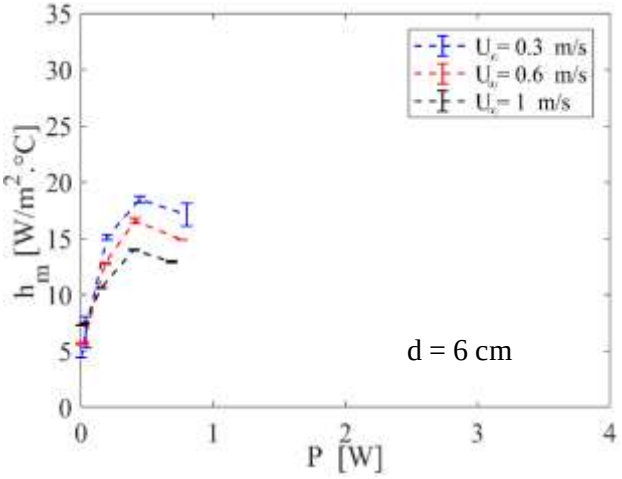

299

300 ***Figure 7.*** *Evolution of the mean heat transfer coefficient (h_m) as a function of power consumption in*
301 *longitudinal wire configuration*

302

303 As the cases of forced convection without EHD correspond to P = 0 W, **Fig.6** and **Fig.7**
304 confirm first of all the benefit of EHD to enhance the heat transfer coefficient in all the
305 studied configurations. Moreover, the mean heat transfer enhancement due to EHD was, as
306 expected, significant at low primary air flow velocity in most cases. Whatever the inter-
307 electrode gap, the primary air flow velocity value of $U_\infty = 0.3$ *m/s* provided a greater value of
308 the mean heat transfer coefficient h_m as compared to other velocities. At this low value of U_∞,
309 inertial forces are reduced and electrostatic forces take over.

310 The influence of the electrode gap also clearly appears on these figures. At the lowest value of
311 *d*, the primary air flow velocity had no influence on the heat transfer coefficient. Electrostatic
312 forces were so high that they generated an impinging jet that blocked the primary air flow. It can
313 also be noticed that the power consumption in all cases was slightly higher when the electrode
314 gap was set to *4 cm*. In one hand, the maximum voltage was limited to *9 kV* for *d = 2 cm* due
315 to potential arcing. On the other hand, the ions collected by the plate for *d = 6 cm* were lower
316 than for *d = 4 cm* due to the increased wire-electrode distance.

317 From **Fig.6**, the optimal configuration in the cross-wire configuration is selected for the
318 primary air flow velocity of *0.3 m/s* and an electrode gap set to *6 cm*. It offered the largest
319 heat transfer coefficient (h_m=34.6 W.m^{-2}.K^{-1}) corresponding to an intensification of the mean
320 heat exchange of the order of 8 times greater than the case of forced convection without EHD.
321 Moreover, this maximum of heat transfer enhancement was obtained with a low value of the
322 electric power (P=1.68 W).

From **Fig.7**, the optimal configuration in the longitudinal wire case is selected also for the primary air flow velocity of *0.3 m/s* but for the electrode gap of *4 cm*. This case allowed to reach a high heat transfer coefficient (h_m =30.9 W.m^{-2}.K^{-1}) which was 7 times greater than the case without EHD, with a low electric power (P = 1.66 W). It can be noticed that at the larger electrode gap (*d = 6 cm*), the heat transfer enhancement was relatively small and presented a peak value at the intermediate electric power. This is due to the fact that the origin of the jet generated by the ionic wind was far from the plate. The jet then expanded beyond this latter, was more spread out and had a lower cooling effect. All these results confirmed the need to investigate the modification of the flow pattern by the ionic wind.

3.2. Flow structure

In this section, the dynamic behavior of the flow structures involved in heat transfer intensification were investigated. Cross wire and longitudinal configurations with *d = 4 cm* and U_∞ *= 0.3 m/s* were firstly analyzed and compared. For both configurations at *V = 16 kV*, the values of the heat transfer coefficients were similar: h_m *= 25 W.m^{-2}.K^{-1}*.

3.2.1. Cross wire configuration

PIV measurement was performed in a plan positioned parallel to the primary air flow and perpendicular to the wire electrode located at distance L_x*=1/2* L_p. **Fig.8-a** displays the mean velocity field and **Fig.8-b** both the streamlines mapping and U_z velocity.

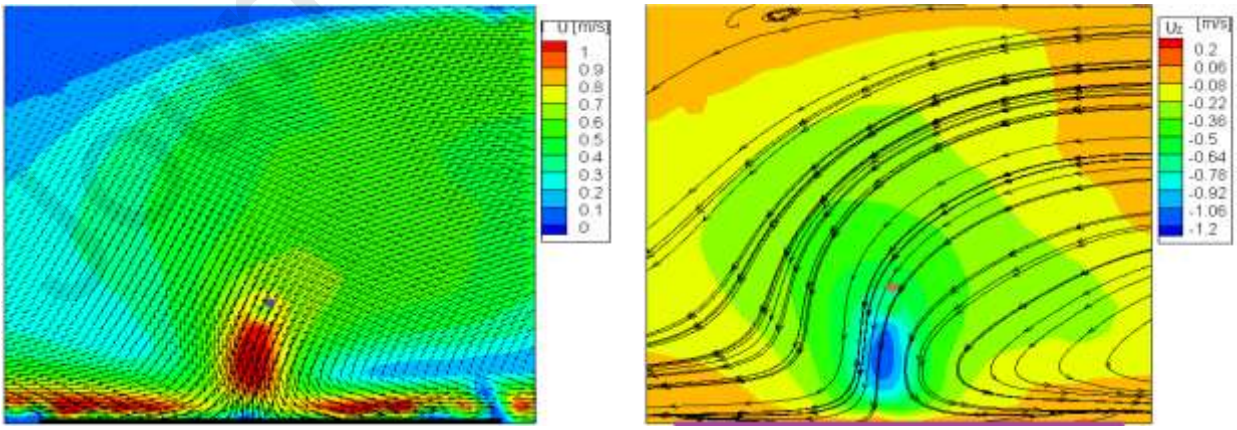

***a**) Mean velocity field U* ***b**) Streamlines and velocity contour U_z*

Figure 8**. Mapping of mean velocity field U **(a)** and streamlines velocity contour of U_z component **(b)

Fig.8 illustrates the mappings of the flow generated by EHD combined with primary air flow directed from right to left. In the investigation area, it is clearly shown that the bulk flow, strongly altered by electrostatic forces, has been modified. It has taken the shape of an air jet that impinges the plate on an area located underneath the wire and then expands in both sides. Furthermore, the IR images previously shown in **Fig.5** demonstrates that intense cooling took place specifically in the area underneath the wire. It is obvious from **Fig.8a** that the velocity component "U_z" had a major effect for cooling the plate. Consequently, the use of the velocity component "U_z" was considered as a relevant criterion of characterization that can be very appropriate to obtain a link with the heat transfer coefficient.

The effect of the primary flow velocity on the flow pattern neighboring the plate was investigated. **Fig.9** displays the contour maps showing the value of the "U_z" component and the streamlines for varying primary flow velocities.

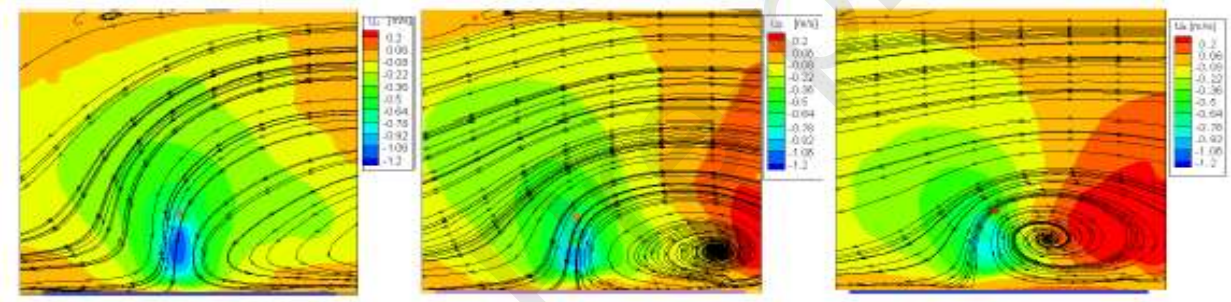

a) $U_\infty = 0.3$ *m./s* ***b)*** $U_\infty = 0.6$ *m./s* ***c)*** $U_\infty = 1$ *m./s*

Figure 9. *U_z contour mapping and streamlines for varying primary flow velocities:* ***a)*** $U_\infty = 0.3$ *m./s,* ***b)*** $U_\infty = 0.6$ *m./s,* ***c)*** $U_\infty = 1$ *m./s*

When analyzing the velocity field mapping of the U_z component, it can be seen that the maximum values of $|U_z|$, about *1 m/s*, was localized in the air jet zone underneath the wire and decreased with the increase of the primary flow velocity as described by many authors [50], [4]. For a primary flow velocity of *0.3 m/s*, the air jet was clearly visible and directed from the wire to the plate. By increasing the primary flow velocity to *0.6 m/s*, the air jet was driven downstream of the plate. A flow vortex could be clearly recognized at the leading edge of the plate in the investigation area (**Fig.9-b)**. By increasing again the primary flow velocity to *1 m/s* as shown in **Fig.9-c**, the primary flow became dominant making the air jet less relevant but still existing. As a result, the center of the vortex moved towards the jet location and blocked the upstream half-zone of the plate. A similar flow structure was obtained for the other electrode gaps set to $d = 2$ *cm* and $d = 6$ *cm*. Therefore, the evolution of the flow structures when varying the primary velocity for these cases can be explained in the same way.

For a deeper analysis, the velocity profiles of the U_z component were plotted along the line ***1*** shown in **Fig.10**. This line parallel to the x-axis is located at distance $z = 1\ cm$ above the plate in such a way to be as much as possible close to the plate while keeping a threshold distance away from the surface plate to avoid laser reflections.

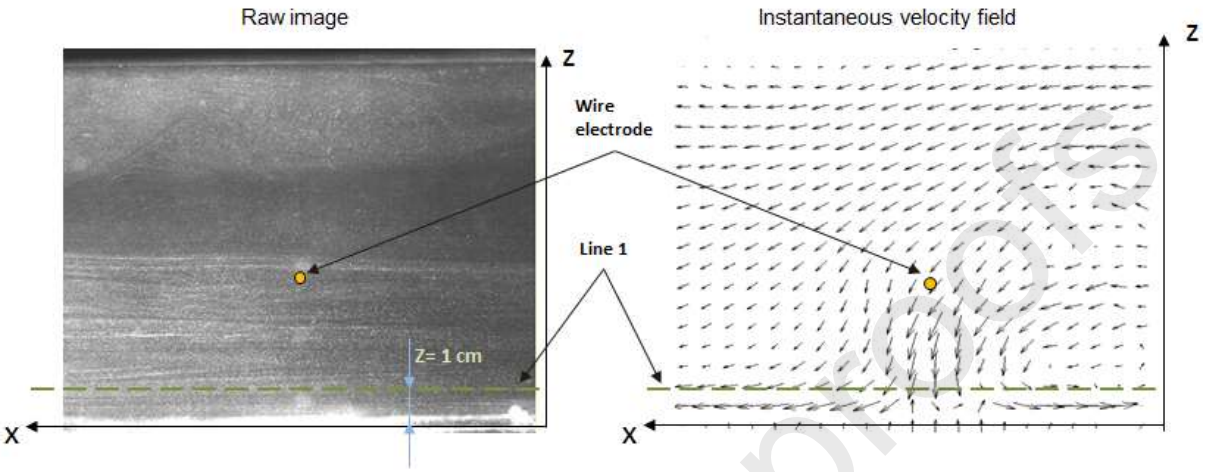

Figure 10. *Position of the line 1 on the x z plan (cross-wire configuration, d = 4 cm)*

Fig.11 illustrates the variation of vertical component of primary flow velocity, U_z, lengthwise the **line 1** as a function of the non-dimensional distance of the plate length, L_p. Temperature profiles resulting from infrared thermography measurement were used to support the dynamic flow characterization as shown in **Fig.12**. Please note that the sharp peaks depicted in **Fig.12** are measurement artefacts as they correspond to the reflection of the wire observed by IR camera.

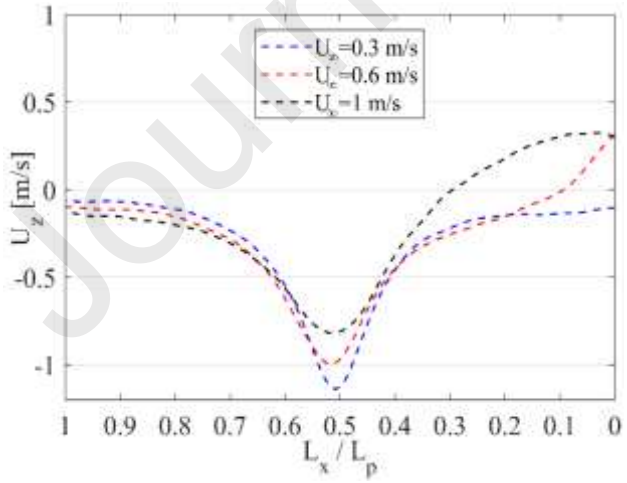

Figure 11. *Velocity component U_z, along the line 1*

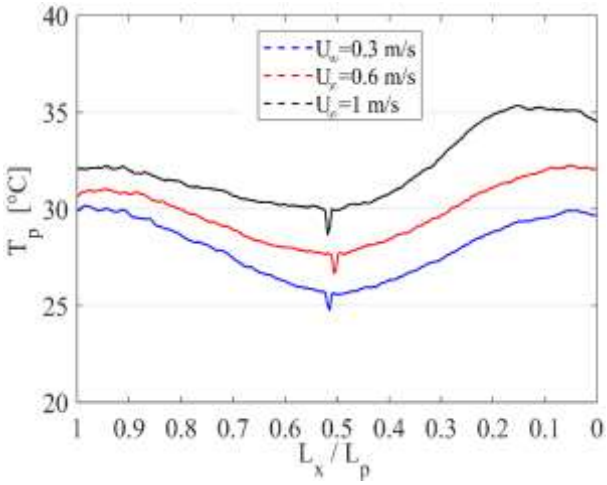

Figure 12. *Surface temperature profiles T_p*

Results show that $|U_z|$ reached its maximum value in the area located just underneath the wire (L_x = 1/2 L_p). When increasing the primary flow velocity from 0.3 to 1 m/s, the magnitude of $|U_z|$ component decreased. Increasing the primary flow velocity disrupted and weakened the secondary flow that initially impinged the plate. The maximum $|U_z|$ for primary flow velocity of 0.3, 0.6 and 1 m/s were 1.2, 1 and 0.7 m/s, respectively. The location of maximum $|U_z|$ also experienced a shift to the left side of plate from the original position at L_x=*1/2* L_p.

For U_∞ = *0.3 m/s*, U_z values remained negative in the whole range over the line 1. The N_{EHD} number was equal to 7.56 in this case. It was also observed that the increase in the primary flow velocity for U_∞ = *0.6 m/s* leads to the appearance of the positive values of the U_z component at the leading edge of the plate. Thus, the effect of the recirculation flow structures on the plate, shown in **Fig.9,** became less relevant. As a result, the N_{EHD} number decreased due to the decrease of the electrostatic forces to the detriment of the inertial forces. The N_{EHD} number was calculated to be 3.22**.** By increasing the primary flow velocity to U_∞ = *1 m/s*, the area of positive U_z component shifted to the left illustrating the driving of the recirculation by the primary flow. This reduced the N_{EHD} to a value of 2.10.

These profiles of the U_z component describe perfectly the surface temperatures distribution of the plate surface, as shown in **Fig. 12**. In this figure, the plate surface temperature profile, T_p, was measured on a line, which is projected from line 1 on *xy* plane (L_x = *1/2* L_p*)*. The cooling of the plate was significant underneath the wire due to high values of $|U_z|$. Based on these results, it can be concluded that the higher $|U_z|$ the better heat transfer intensification. Therefore, the highest amount of heat transfer exchange could be expected to be achieved at U_∞ = *0.3 m/s*.

Similar behaviors were obtained *d = 2 cm* and *d = 6 cm* concerning the evolutions of the U_z component and the temperature profiles. These results confirm those obtained on the convective heat transfer coefficient measurement by infrared thermography, where it has been shown that maximum heat transfer coefficient was achieved for the lowest primary flow velocity value.

To obtain the optimum electrode gap distance, the velocity profiles of U_z component were compared for the optimal primary flow velocity of U_∞ = *0.3 m./s*. **Fig. 13** shows the velocity profiles of U_z component along line 1 for different electrode gaps.

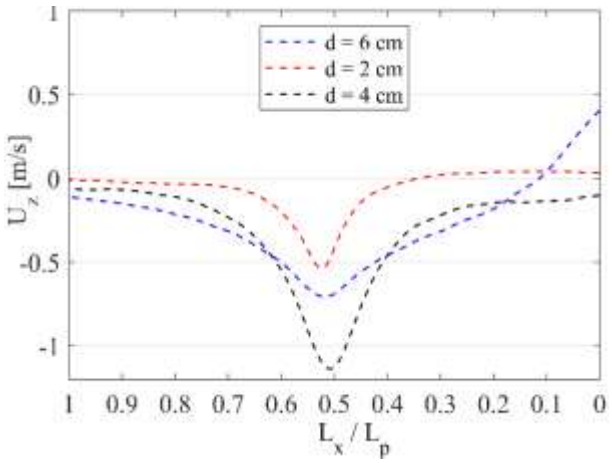

Figure 13. *U_z component profiles, along line 1 for primary flow velocity of U_∞ = 0.3 m./s at different electrode gaps.*

From **Fig.13**, it appears that, compared to cases *d = 4 cm* and *d = 6 cm*, the case of *d = 2 cm* had the lowest values of $|U_z|$, because in this case the voltage was limited to 9 kV to avoid arcing phenomenon.

At wire position of L_x= *1/2* L_p, and when *d = 4 cm*, the U_z component profile was characterized by high values compared to the case when *d = 6 cm* which resulted in a greater heat transfer intensification. However, for *d = 6 cm* it can be noticed that in areas located upstream and downstream the wire, the U_z profile component was more spread out and exhibited greater values comparing to the case where *d = 4cm*. Therefore, if the local heat transfer underneath the wire was better for *d = 4 cm*, the configuration with *d = 6 cm* gave rise to the highest average heat transfer coefficient (**Fig.6c**). These results show the necessity to take into account other aspects related to process application (homogeneous treatment vs local treatment) to conclude on both cases regarding the optimal heat transfer intensification case.

3.2.2. Longitudinal wire configuration

For the case of longitudinal wire configuration, PIV measurement was carried out basically in the two distinct planes, *xz* and *yz* at positions of L_y = *1/2* L_p and L_x = *1/2* L_p, respectively.

The analysis focused on the optimal configuration *(d = 4 cm, U_∞ = 0.3 m/s)* giving rise to a maximum mean heat transfer coefficient $h_m = 25\ W.m^{-2}.K^{-1}$.

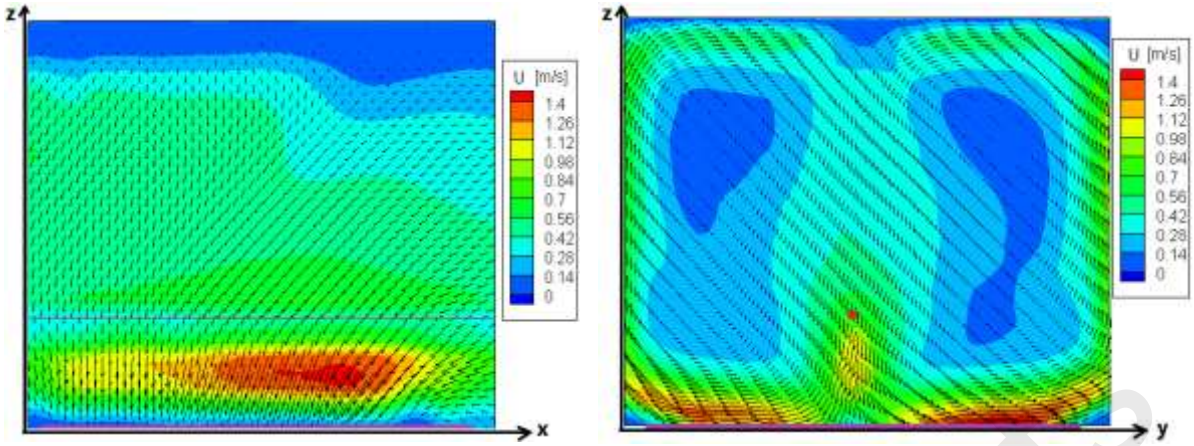

a) *Mapping in xz plane* ***b)*** *Mapping in yz plane*

Figure. 14 *Mean velocity vector and contour mapping for the optimal configuration in: a) in xz plane and b) yz plane*

Fig.14 shows the mean velocity vector field in *xz* and *yz* plane. As shown in both planes, the EHD-generated flow combined with the primary air flow formed an air jet that impinged the plate. The air jet was located along the plate, underneath the wire (**Fig.14-a**) and formed two parietal jets developing on both sides of impinging zone (**Fig.14-b**). As a result, both velocity components U_z and U_y could be considered as the most relevant components influencing the cooling of the plate.

Therefore, in longitudinal wire configuration, one can consider the velocity component along *y* axis, U_y, as a relevant means of characterization in addition to U_z. For a better exploitation of U_y and U_z, the **line 2** displayed in **Fig.15** was used as reference for plotting the velocity profiles.

PIV measurement conducted in the *yz* plane, shown in **Fig.15**, reveals that the $|U_y|$ component presented relatively high values in an area very close to the plate on both sides the air jet. Therefore, the U_y component of the spreading air jet might have a major influence on cooling effect, say heat transfer intensification, on both sides of the plate.

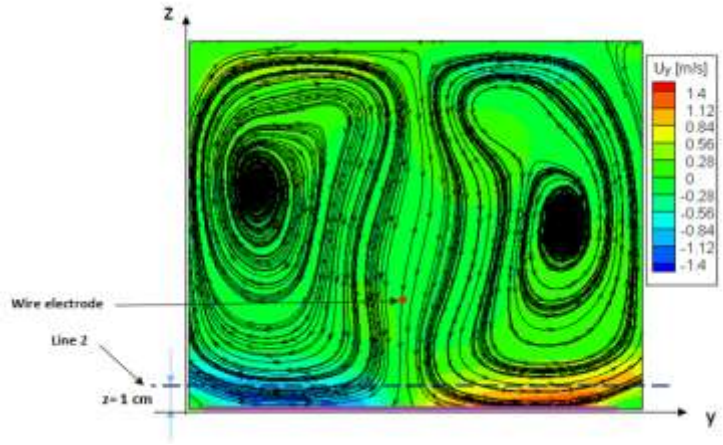

451 ***Figure .15*** *Mapping of the U_y contours component and streamlines in xz plan*

452

453 It was found previously in **Fig.5** that, for longitudinal wire configuration, the cooling of the
454 plate along the wire was more homogeneous for *d = 4 cm*. This tendency might be explained
455 by the change in the vortices shape structures of the secondary flow (swirl) along the plate.

456 To better understand the evolution of the flow structures, PIV measurements were carried out
457 in the *yz* plane at different positions along the *x* axis: Position 1: $L_x = 1/4\ L_p$, Position 2: $L_x = 1/2\ L_p$, and Position 3: $L_x = 3/4\ L_p$. The mapping of the streamlines and the velocity profiles of
459 both U_y and U_z components lengthwise **line2** are shown in **Fig.16** and **Fig.17**, respectively.

460

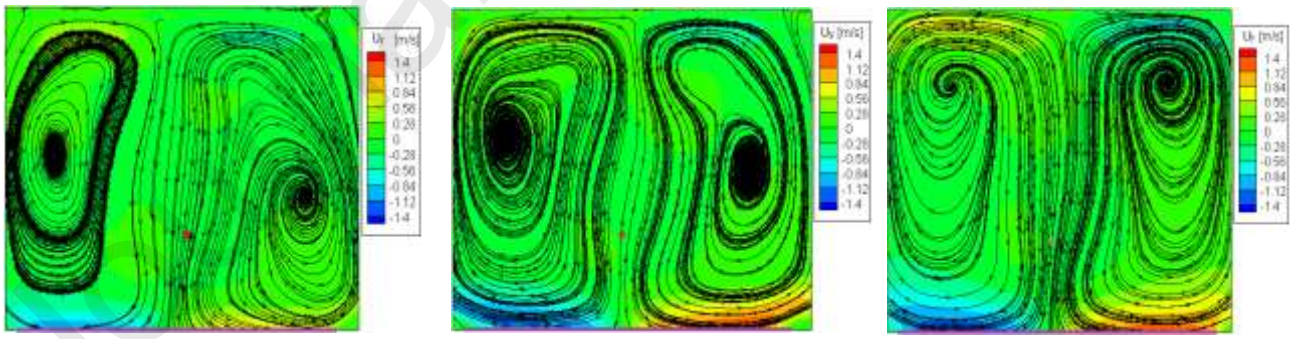

$L_x = 1/4\ L_p$ $L_x = 1/2\ L_p$ $L_x = 3/4\ L_p$

Figure. 16 *Mapping of the U_y contours component and streamlines on the yz plan at positions:* ***(a)*** $L_x = 1/4\ L_p$, ***(b)*** $L_x = 1/2\ L_p$ *and* ***(c)*** $L_x = 3/4\ L_p$

461

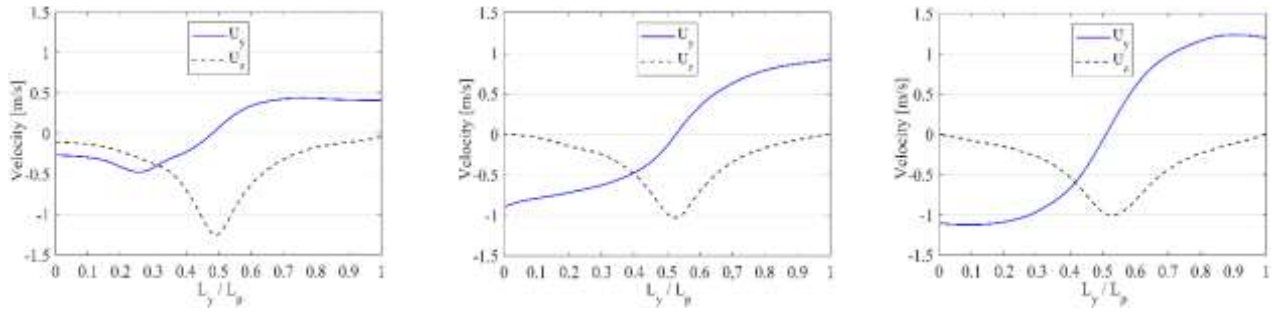

a) $L_x = 1/4\ L_p$ ***b)*** $L_x = 1/2\ L_p$ ***c)*** $L_x = 3/4\ L_p$

Figure. 17 *Velocity profiles component of U_z and U_y lengthwise line 2 on the yz plan at positions:* ***(a)*** $L_x = 1/4\ L_p$, ***(b)*** $L_x = 1/2\ L_p$ *and* ***(c)*** $L_x = 3/4\ L_p$

According to the streamlines cartography displayed in **Fig.16,** it can be noticed that the vortices centers increased in height along the *x* axis. The velocity profile of U_y component plotted along **line 2** shows that the amplitude of U_y increased from *0.3 m/s* at the first plane to *1.2 m/s* at the last plane (**Fig.17c**). As the primary flow passed over the plate, it interacted with the EHD air jet to form two growing counter-rotating vortices. This growth resulted in the increase of transverse velocity, U_y in the direction of the primary flow (x axis). **Fig.17** also shows the profiles of U_z component plotted on **line 2**. This figure illustrates that the maximum absolute values decreased along the plate from *1.3 m/s* at $L_x = 1/4\ L_p$ to *0.6 m/s* at $L_x = 3/4\ L_p$. This tendency was confirmed with the results shown in **Fig.18**. The measurement performed on *xz* plane, at $z = 1\ cm$ shows that position $L_x = 1/4\ L_p$ was characterized by the maximum velocity value of $|U_z|$. The results shown in **Fig.18**, explain clearly the concordance between the evolution of the U_z velocity component and the surface plate temperature profile presented in **Fig.19**: the minimum surface plate temperature, close to *30 °C*, occurred at $L_x = 0.4\ L_p$ where vertical component of velocity reached its maximum, $|U_z| = 1.3\ m/s$. Similar behavior discussed in **Figs.18-19** was observed for other electrode gap values, $d = 2\ cm$ and $d = 6\ cm$, but with different magnitudes.

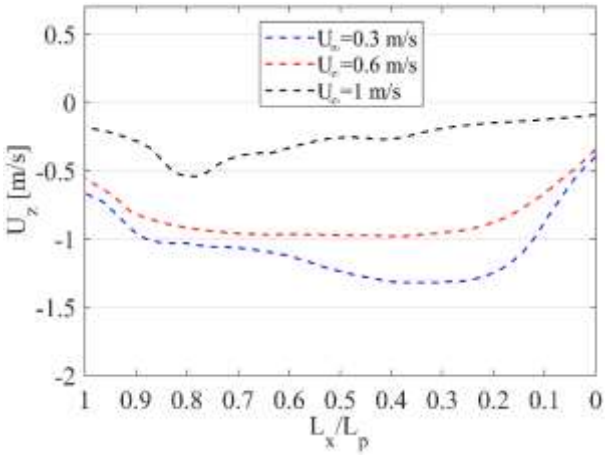

Figure 18. *Velocity profiles of U_z component, along a line located at z = 1 cm in xz plane*

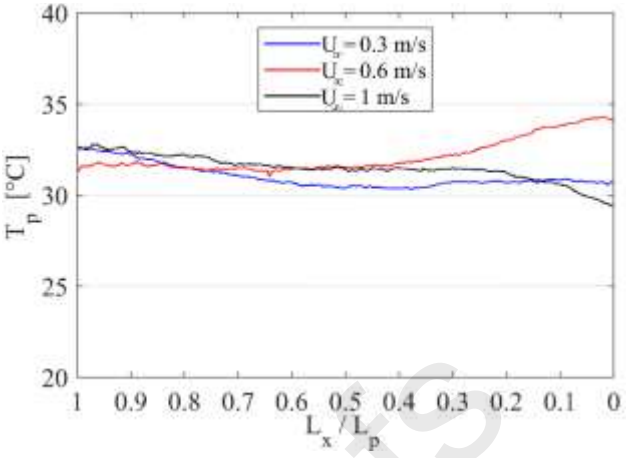

Figure 19*. Surface temperature profiles T_p , just beneath the wire*

4. Conclusion

The present study is one of the first where both PIV and IR thermography were performed to investigate the heat transfer enhancement by ionic wind in a rectangular channel, which dimensions correspond to real size of potential future drying systems.

The experiments clearly demonstrated that such an approach is necessary to understand, in different wire-to plate electrode configurations, the results of heat transfer enhancement versus flow structure alteration.

Thermal characterization essentially made possible to identify and select optimal configurations according to different aspects like transfer enhancement, thermal homogeneity and energy consumption. The study of flow characterization by PIV figured out the relationship between the geometric and operating parameters with the heat transfer intensification distribution. It enabled the understanding of the mechanisms of secondary flows structures combined with the primary flow (air jet, vortex...). The following conclusions were derived:

In all cases, the highest heat transfer enhancement by EHD was obtained for the smaller primary air flow velocity (0.3 *m/s*). As expected, at low Reynolds number, primary air flow provided the most efficient use of the secondary air flow induced by EHD. This in fact corresponds to a large EHD number.

For the single wire-electrode arranged perpendicular to the primary air flow, the greatest increase in heat transfer occurred when the wire-electrode was set at the highest distance from the plate

($d = 6\ cm$) where it provided the best intensification ($h_m/h_0 = 8$). For the minimum value of wire to plate distance, the heat transfer enhancement was localized over a very limited area beneath the wire. In this case, the generated secondary flow was similar to an impinging jet that caused a strong intensification on an area located beneath the wire. Such a configuration should be selected when the objective consists in getting local heat/mass transfer enhancement without any necessity to get homogeneous treatment.

For the case of single wire-electrode arranged parallel to primary air flow, the highest increase in heat transfer enhancement was achieved for wire to plate distance of 4 cm which provided the most efficient combination of primary and secondary air flow where the intensification was improved 7 times ($h_m/h_0 = 7$). In this case, the air jet was generated along the wire where the maximum velocity was similar to that achieved with the cross wire. It was shown that contra-rotating vortices appeared and were developing as progressing in the channel. Such a configuration should be selected when the objective consists in getting an homogeneous treatment due the change in the vortices shape structures of the secondary flow along the plate.

Whatever the configuration, results indicated that such a deep analysis of heat transfer enhancement and flow structure is required for a correct design of future system (geometrical parameters and applied voltage) according to the objective. High local enhancement can be reached when decreasing the electrode gap but the enhancement is then limited by arcing phenomenon. A more homogeneous enhancement requires a larger inter-electrodes gap that lead to a larger jet with lower impacting velocities.

Acknowledgement

Acknowledgement to Mohammad Javad Javaherian (Ph.D. candidate at the Department of Aerospace & Ocean Engineering, Virginia Tech, USA) for providing language help with this manuscript. The authors gratefully acknowledge the support of the Pays de Loire program for outstanding research in the field of energetics (PERLE2).

References

[1] H. Omidvarborna, M. Dasht-e-Bayz, A. Mehrabani-Zeinabad, M. Nasr Esfahany, Effect of applied EHD on in-tube condensation of R-134a within an assembled

experimental rig including a laboratory heat exchanger, Exp. Therm. Fluid Sci. 58 (2014) 112–120. https://doi.org/10.1016/j.expthermflusci.2014.06.007.

[2] S.W. Ahmad, T.G. Karayiannis, D.B.R. Kenning, A. Luke, Compound effect of EHD and surface roughness in pool boiling and CHF with R-123, Appl. Therm. Eng. 31 (2011) 1994–2003. https://doi.org/10.1016/j.applthermaleng.2011.03.005.

[3] R.T. Huang, W.J. Sheu, C.C. Wang, Heat transfer enhancement by needle-arrayed electrodes - An EHD integrated cooling system, Energy Convers. Manag. 50 (2009) 1789–1796. https://doi.org/10.1016/j.enconman.2009.03.017.

[4] S. Ould Ahmedou, M. Havet, Effect of Process Parameters on the EHD Airflow, J. Electrostat. 67 (2009) 222–227. https://doi.org/https://doi.org/10.1016/j.elstat.2009.01.055.

[5] T.G. Karayiannis, EHD boiling heat transfer enhancement of R123 and R11 on a tube bundle, Appl. Therm. Eng. 18 (1998) 809–817. https://doi.org/10.1016/S1359-4311(97)00102-6.

[6] E. Bardy, M. Hamdi, M. Havet, O. Rouaud, Transient exergetic efficiency and moisture loss analysis of forced convection drying with and without electrohydrodynamic enhancement, Energy. 89 (2015) 519–527. https://doi.org/10.1016/j.energy.2015.06.017.

[7] N. Benard, P. Braud, G. Touchard, E. Moreau, Detachment and attachment of an axisymmetric non-reactive jet with turbulent shear layer: Control by plasma actuator, Exp. Therm. Fluid Sci. 32 (2008) 1193–1203. https://doi.org/https://doi.org/10.1016/j.expthermflusci.2008.01.010.

[8] N. Monrolin, F. Plouraboué, O. Praud, Electrohydrodynamic thrust for in-atmosphere propulsion, AIAA J. 55 (2017) 4296–4305. https://doi.org/10.2514/1.J055928.

[9] K. Smith, G. Byrne, R. Kempers, A.J. Robinson, Electrohydrodynamic augmentation of a reflux thermosyphon, Exp. Therm. Fluid Sci. 79 (2016) 175–186. https://doi.org/10.1016/j.expthermflusci.2016.07.003.

[10] B. Kim, S. Lee, Y.S. Lee, K.H. Kang, Ion wind generation and the application to cooling, J. Electrostat. 70 (2012) 438–444. https://doi.org/10.1016/j.elstat.2012.06.002.

[11] A.M. Gañán-Calvo, J. Dávila, A. Barrero, Current and droplet size in the electrospraying of liquids. Scaling laws, J. Aerosol Sci. 28 (1997) 249–275. https://doi.org/10.1016/S0021-8502(96)00433-8.

[12] N. Zouzou, E. Moreau, Effect of a filamentary discharge on the particle trajectory in a plane-to-plane DBD precipitator, J. Phys. D. Appl. Phys. 44 (2011) 285204. https://doi.org/10.1088/0022-3727/44/28/285204.

[13] J. Chen, J.H. Davidson, Electron Density and Energy Distributions in the Positive DC Corona: Interpretation for Corona-Enhanced Chemical Reactions, Plasma Chem. Plasma Process. 22 (2002) 199–224. https://doi.org/10.1023/A:1014851908545.

[14] L. Léger, E. Moreau, G. Touchard, Control of low velocity airflow along a flat plate with a DC electrical discharge, in: Conf. Rec. 2001 IEEE Ind. Appl. Conf. 36th IAS Annu. Meet. (Cat. No.01CH37248), 2001: pp. 1536–1543 vol.3. https://doi.org/10.1109/IAS.2001.955739.

[15] G. Artana, J. D'adamo, L. Léger, E. Moreau, G. Touchard, Flow control with electrohydrodynamic actuators, AIAA J. 40 (2002) 1773–1779. https://doi.org/10.2514/2.1882.

[16] H.R. Velkoff, R. Godfrey, Low-velocity heat transfer to a flat plate in the presence of a corona discharge in air, J. Heat Transfer. 101 (1979) 157–163. https://doi.org/10.1115/1.3450907.

[17] Y. Tada, A. Takimoto, Y. Hayashi, Heat Transfer Enhancement in a Convective Field by Applying Ionic Wind, J. Enhanc. Heat Transf. 4 (1997) 71–86. https://doi.org/10.1615/JEnhHeatTransf.v4.i2.20.

[18] D.B. Go, R. a. Maturana, T.S. Fisher, S. V. Garimella, Enhancement of external forced convection by ionic wind, Int. J. Heat Mass Transf. 51 (2008) 6047–6053. https://doi.org/10.1016/j.ijheatmasstransfer.2008.05.012.

[19] P.Y. Wang, J.M. Liu, Z.H. Liu, Y.J. Chen, Experiment and simulation of natural convection heat transfer of transformer oil under electric field, Int. J. Heat Mass Transf. 115 (2017) 441–452. https://doi.org/10.1016/j.ijheatmasstransfer.2017.07.069.

[20] H.M. Deylami, Effects of EHD on the flow and heat transfer characteristics in a

rectangular corrugated channel, Heat Mass Transf. 55 (2019) 3711–3720. https://doi.org/10.1007/s00231-019-02693-z.

[21] N. Kasayapanand, Electrode arrangement effect on natural convection, Energy Convers. Manag. 48 (2007) 1323–1330. https://doi.org/10.1016/j.enconman.2006.09.022.

[22] H.M. Deylami, N. Amanifard, F. Dolati, R. Kouhikamali, K. Mostajiri, Numerical investigation of using various electrode arrangements for amplifying the EHD enhanced heat transfer in a smooth channel, J. Electrostat. 71 (2013) 656–665. https://doi.org/10.1016/j.elstat.2013.03.007.

[23] T. Mizushina, H. Ueda, T. Matsumoto, K. Waga, Effect of electrically induced convection on heat transfer of air flow in an annulus, J. Chem. Eng. JAPAN. 9 (1976) 97–102. https://doi.org/10.1252/jcej.9.97.

[24] S. Wangnipparnto, J. Tiansuwan, S. Jiracheewanun, T. Kiatsiriroat, C.C. Wang, Air side performance of thermosyphon heat exchanger in low Reynolds number region: With and without electric field, Energy Convers. Manag. 43 (2002) 1791–1800. https://doi.org/10.1016/S0196-8904(01)00136-4.

[25] S. Wangnipparnto, J. Tiansuwan, T. Kiatsiriroat, C.C. Wang, Performance analysis of thermosyphon heat exchanger under electric field, Energy Convers. Manag. 44 (2003) 1163–1175. https://doi.org/10.1016/S0196-8904(02)00104-8.

[26] D. Nakhla, H. Sadek, J.S. Cotton, Melting performance enhancement in latent heat storage module using solid extraction electrohydrodynamics (EHD), Int. J. Heat Mass Transf. 81 (2015) 695–704. https://doi.org/10.1016/j.ijheatmasstransfer.2014.10.016.

[27] L. Shi, D.J. Bayless, G. Kremer, B. Stuart, Numerical investigation of the flow profiles in the electrically enhanced cyclone, J. Air Waste Manag. Assoc. 57 (2007) 489–496. https://doi.org/10.3155/1047-3289.57.4.489.

[28] A. Rafiei-Siahestalkhi, N. Amanifard, H.M. Deylami, F. Dolati, Numerical Investigation of Electrohydrodynamic Forced Convection Heat Transfer from a Circular Cylinder, Heat Transf. Eng. (2021) 2021. https://doi.org/10.1080/01457632.2021.1896837.

[29] M.M. Ohadi, D.A. Nelson, S. Zia, Heat transfer enhancement of laminar and turbulent pipe flow via corona discharge, Int. J. Heat Mass Transf. 34 (1991) 1175–1187. https://doi.org/10.1016/0017-9310(91)90026-B.

[30] I.Y. Chen, C.J. Chen, C.C. Wang, Influence of electrode configuration on the heat transfer performance of a LED heat source, Int. J. Heat Mass Transf. 77 (2014) 795–801. https://doi.org/10.1016/j.ijheatmasstransfer.2014.06.023.

[31] M. Molki, T. Harirchian, The enhancement effect of corona discharge on natural convection heat transfer in triangular channels, in: Am. Soc. Mech. Eng. Heat Transf. Div. HTD, Orlando, Florida, USA, 2005: pp. 477–487. https://doi.org/10.1115/IMECE2005-80070.

[32] F. Asadzadeh, M. Nasr Esfahany, N. Etesami, Natural convective heat transfer of Fe 3O 4/ethylene glycol nanofluid in electric field, Int. J. Therm. Sci. 62 (2012) 114–119. https://doi.org/10.1016/j.ijthermalsci.2011.11.010.

[33] Y.X. Bai, B. Sun, Study of electrohydrodynamic (EHD) drying technique for shrimps, J. Food Process. Preserv. 35 (2011) 891–897. https://doi.org/10.1111/j.1745-4549.2011.00542.x.

[34] S. Taghian Dinani, M. Havet, The influence of voltage and air flow velocity of combined convective-electrohydrodynamic drying system on the kinetics and energy consumption of mushroom slices, J. Clean. Prod. 95 (2015) 203–211. https://doi.org/10.1016/j.jclepro.2015.02.033.

[35] F.C. Lai, A prototype of EHD-enhanced drying system, J. Electrostat. 68 (2010) 101–104. https://doi.org/10.1016/j.elstat.2009.08.002.

[36] F.C. Lai, K. Tay, Electrohydrodynamically-enhanced forced convection in a horizontal channel with oscillatory flows, Heat Transf. Eng. 31 (2010) 147–156. https://doi.org/10.1080/01457630903285427.

[37] M. Yang, C. Ding, Electrohydrodynamic (EHD) drying of the Chinese wolfberry fruits, Springerplus. 5 (2016) 40064. https://doi.org/10.1186/s40064-016-2546-1.

[38] T. Defraeye, A. Martynenko, Electrohydrodynamic drying of multiple food products: Evaluating the potential of emitter-collector electrode configurations for upscaling, J.

Food Eng. 240 (2019) 38–42. https://doi.org/10.1016/j.jfoodeng.2018.07.011.

[39] S. Taghian Dinani, M. Havet, N. Hamdami, M. Shahedi, Drying of Mushroom Slices Using Hot Air Combined with an Electrohydrodynamic (EHD) Drying System, Dry. Technol. 32 (2014) 597–605. https://doi.org/10.1080/07373937.2013.851086.

[40] F.C. Lai, D.S. Wong, EHD-Enhanced Drying with Needle Electrode, Dry. Technol. 21 (2003) 1291–1306. https://doi.org/10.1081/DRT-120023181.

[41] N.N. Barthakur, T. Al-Kanani, An Electrohydrodynamic Technique for Removal of Moisture from Soil Samples, Commun. Soil Sci. Plant Anal. 21 (1990) 649–665. https://doi.org/10.1080/00103629009368260.

[42] C. Zhong, A. Martynenko, P. Wells, K. Adamiak, Numerical investigation of the multi-pin electrohydrodynamic dryer: Effect of cross-flow air stream, Dry. Technol. 37 (2019) 1665–1677. https://doi.org/10.1080/07373937.2018.1531291.

[43] F.C. Lai, R.K. Sharma, EHD-enhanced drying with multiple needle electrode, J. Electrostat. 63 (2005) 223–237. https://doi.org/10.1016/j.elstat.2004.10.004.

[44] A. Polat, N. Izli, Determination of drying kinetics and quality parameters for drying apricot cubes with electrohydrodynamic, hot air and combined electrohydrodynamic-hot air drying methods, Dry. Technol. 0 (2020) 1–16. https://doi.org/10.1080/07373937.2020.1812633.

[45] A. Martynenko, T. Kudra, J. Yue, Multipin EHD dryer: Effect of electrode geometry on charge and mass transfer, Dry. Technol. 35 (2017). https://doi.org/10.1080/07373937.2017.1285311.

[46] L.W. Da Silva, M. Molki, M.M. Ohadi, Electrohydrodynamic enhancement of R-134a condensation on enhanced tubes, Conf. Rec. - IAS Annu. Meet. (IEEE Ind. Appl. Soc. 2 (2000) 757–764. https://doi.org/10.1109/IAS.2000.881915.

[47] K. Brand, J. Seyed-Yagoobi, Experimental study of electrohydrodynamic induction pumping of a dielectric micro liquid film in external horizontal condensation process, J. Heat Transfer. 125 (2003) 1096–1105. https://doi.org/10.1115/1.1621890.

[48] H. Sadek, A.J. Robinson, J.S. Cotton, C.Y. Ching, M. Shoukri, Electrohydrodynamic enhancement of in-tube convective condensation heat transfer, Int. J. Heat Mass

Transf. 49 (2006) 1647–1657. https://doi.org/10.1016/j.ijheatmasstransfer.2005.10.030.

[49] A. Bryszewska-Mazurek, W. Mazurek, The influence of electric field on HFC-245fa condensation, Mater. Sci. Pol. 27 (2009) 1257–1261.

[50] Y. Liu, R. Li, F. Wang, H. Yu, The effect of electrode polarity on EHD enhancement of boiling heat transfer in a vertical tube, Exp. Therm. Fluid Sci. 29 (2005) 601–608. https://doi.org/10.1016/j.expthermflusci.2004.07.004.

[51] J. Cotton, A.J. Robinson, M. Shoukri, J.S. Chang, A two-phase flow pattern map for annular channels under a DC applied voltage and the application to electrohydrodynamic convective boiling analysis, Int. J. Heat Mass Transf. 48 (2005) 5563–5579. https://doi.org/10.1016/j.ijheatmasstransfer.2005.05.032.

[52] G. McGranaghan, A.J. Robinson, EHD augmented convective boiling: Flow regimes and enhanced heat transfer, Heat Transf. Eng. 35 (2014) 517–527. https://doi.org/10.1080/01457632.2013.833054.

[53] S. Siedel, S. Cioulachtjian, A.J. Robinson, J. Bonjour, Electric field effects during nucleate boiling from an artificial nucleation site, Exp. Therm. Fluid Sci. 35 (2011) 762–771. https://doi.org/10.1016/j.expthermflusci.2010.06.006.

[54] Y.Q. Zu, Y.Y. Yan, A numerical investigation of electrohydrodynamic (EHD) effects on bubble deformation under pseudo-nucleate boiling conditions, Int. J. Heat Fluid Flow. 30 (2009) 761–767. https://doi.org/10.1016/j.ijheatfluidflow.2009.03.008.

[55] N.N. Barthakur, Electrohydrodynamic enhancement of evaporation from NaCl solutions, Desalination. 78 (1990) 455–465. https://doi.org/10.1016/0011-9164(90)80064-I.

[56] X. Quan, M. Gao, P. Cheng, J. Li, An experimental investigation of pool boiling heat transfer on smooth/rib surfaces under an electric field, Int. J. Heat Mass Transf. 85 (2015) 595–608. https://doi.org/10.1016/j.ijheatmasstransfer.2015.01.083.

[57] G. Heidarinejad, R. Babaei, Numerical investigation of electro hydrodynamics (EHD) enhanced water evaporation using Large Eddy Simulation turbulent model, J. Electrostat. 77 (2015) 76–87. https://doi.org/10.1016/j.elstat.2015.07.007.

[58] M. Huang, F.C. Lai, Numerical study of EHD-enhanced water evaporation, J.

706 Electrostat. 68 (2010) 364–370. https://doi.org/10.1016/j.elstat.2010.05.003.

707 [59] Y.H. Diao, Y. Liu, J. Zhang, L. Guo, Y.H. Zhao, S. Wang, Effect of electric field on
708 the enhanced heat transfer characteristic of an evaporator with multilayered sintered
709 copper mesh, J. Electrostat. 73 (2015) 26–32.
710 https://doi.org/10.1016/j.elstat.2014.10.005.

711 [60] S.A. Ould Ahmedou, O. Rouaud, M. Havet, Assessment of the electrohydrodynamic
712 drying process, Food Bioprocess Technol. 2 (2009) 240–247.
713 https://doi.org/10.1007/s11947-008-0078-6.

714 [61] T. Kudra, A. Martynenko, Energy Aspects in Electrohydrodynamic Drying, Dry.
715 Technol. 33 (2015) 1534–1540. https://doi.org/10.1080/07373937.2015.1009540.

716 [62] T. Anukiruthika, J.A. Moses, C. Anandharamakrishnan, Electrohydrodynamic drying
717 of foods: Principle, applications, and prospects, J. Food Eng. 295 (2021) 110449.
718 https://doi.org/10.1016/J.JFOODENG.2020.110449.

719 [63] T. Defraeye, A. Martynenko, Future perspectives for electrohydrodynamic drying of
720 biomaterials, Dry. Technol. 36 (2018) 1–10.
721 https://doi.org/10.1080/07373937.2017.1326130.

722 [64] M. Hamdi, M. Havet, O. Rouaud, D. Tarlet, Comparison of different tracers for PIV
723 measurements in EHD airflow, Exp. Fluids. 55 (2014). https://doi.org/10.1007/s00348-
724 014-1702-z.

725 [65] S.E. Sadek, R.G. Fax, M. Hurwitz, The influence of electric fields on convective heat
726 and mass transfer from a horizontal surface under forced convection, J. Heat Transfer.
727 94 (1972) 144–148. https://doi.org/10.1115/1.3449885.

728 [66] T. Yamamoto, H.R. Velkoff, Electrohydrodynamics in an electrostatic precipitator, J.
729 Fluid Mech. 108 (1981) 1–18. https://doi.org/10.1017/S002211208100195X.

730 [67] F.C. Lai, P.J. McKinney, J.H. Davidson, Oscillatory electrohydrodynamic gas flows, J.
731 Fluids Eng. 117 (1995) 491–497. https://doi.org/10.1115/1.2817289.

732

733

Highlights

- Using EHD in thermal process leads to heat transfer enhancement and reduces energy consumption
- EHD induced secondary flow disturbs the thermal boundary layer and increases heat transfer
- Wire /plate electrode arrangement is efficient for combined secondary flow generation with primary flow in a channel
- Longitudinal wire configuration improves the homogeneity of heat transfer compared to cross wire configuration
- Combination of thermal and dynamic flow characterization is the main key for EHD process optimization